CrossMark

ORIGINAL PAPER

Groundwater control and curtain grouting for tunnel construction in completely weathered granite

Jinquan Liu[1,2] (ID) **· Weizhong Chen[1,3] · Jingqiang Yuan[1] · Changjun Li[1,2] ·
Qingyan Zhang[1,2] · Xiaofei Li[1,2]**

Abstract During tunnel construction, groundwater inrush from completely weathered granite strata is a significant challenge to geotechnical engineers. Up to the present, prevention of water inrushing hazards is almost exclusively based on the experience of engineers. This paper presents a coupled seepage–erosion water inrush model to investigate the characteristics of seepage–erosion properties. The proposed model is based on classical theories of solute transport and fluid dynamics in porous media. In the model, changes of porosity link permeability with the accumulation of particle loss in the seepage–erosion process. The coupled seepage–erosion model was applied to examine the influence of curtain grouting thickness on the seepage–erosion process. The results showed that the seepage–erosion process was attenuated as thickness increased. The results also showed that the porosity and permeability visibly changed and the water inflow clearly exceeded the acceptable engineering criterion when the thickness was less than 6 m. However, with a further increase in thickness, the seepage–erosion process was suppressed and little changes of the relative parameters were showed. The numerical results demonstrated that a curtain grouting thickness of 6 m was suitable for curtain grouting in completely weathered granite. Field investigation of Cenxi

tunnel verified the effectiveness of the thickness determined by the proposed model.

Introduction

In recent years, more than 100 cases of water inrush and mud gushing have been observed during tunnel construction across the globe (Zhao et al. 2013), causing serious casualties and huge economic losses. Among them, a large number of water inrush disasters occurred frequently in completely weathered granite strata. Tunneling in such conditions will be particularly difficult because of the potential for encountering mix face conditions, collapse, and erosion (Zhao et al. 2007; Zhang et al. 2014a; Shirlaw 2016). The complex ground conditions resulting from weathering are challenging for tunnel construction. The weathered rock mass retains relic structure from its geological past, which will often control its engineering behavior (Shirlaw 2016). Under these condition, groundwater inrushing may happened in various tunneling method, e.g. mining tunneling, microtunneling (Ni and Cheng 2012; Shen et al. 2014, 2016), and shield tunneling (Wu et al. 2015a). Over the last 30 years, many researches have been devoted to studying the description, classification, weathering process, and engineering behavior of weathered rocks. Anno (1995) and Arikan et al. (2007) have developed a systematical description and classification of weathered rocks. Irfan (1997) studied the mineralogical characterization and classification of weathered granite. Six grades from fresh rock (Grade I) to residual soil (Grade VI) were adopted to classify weathered

✉ Jinquan Liu
  jinquanliu99@163.com

1   State Key Laboratory of Geomechanics and Geotechnical
    Engineering, Institute of Rock and Soil Mechanics, Chinese
    Academy of Sciences, Wuhan 430071, Hubei, China

2   University of Chinese Academy of Sciences, Beijing 100049,
    China

3   Geotechnical and Structural Engineering Research Center,
    Shandong University, Jinan 250061, Shandong, China

granites. The main minerals include quartz, feldspar, biotite, and hornblende. Weathering results in a loss of feldspar, leaving a material predominantly consisting of quartz particles and clay minerals such as kaolinite and montmorillonite as the weathering grade increases to completely weathered granite (Grade V). This material erodes rapidly and becomes weak and soil-like. Howat (1985) and Gamon (1986) carried on a discussion on "completely weathered granite-soil or rock?", and the shear strength data indicated that the completely weathered granite was more soil than rock, as observed from recently field investigations (Cui et al. 2016; Liu et al. 2016). Shirlaw et al. (2000) also claimed that the completely weathered rocks were prone to erosion when exposed because of little cementation. Under certain conditions, the clay minerals resulting from weathering may be gradually eroded by groundwater flow, leading to the rapid increase of ground permeability and the formation of water path, and ultimately the water inrush disaster. Therefore, it is no exaggeration that water inrush disasters have become a serious threat to tunnel construction in completely weathered granite due to their special engineering behavior. Consequently, in order to control water inrush disasters and improve safety in tunnel construction, it is absolutely necessary to reveal the water inrush mechanism and put forward effective prevention measures for completely weathered granite.

Numerical modeling has the advantage of analyzing the water inflow in various geological conditions, which has been widely used by many researchers (Font-Capó et al. 2011; Zhu and Wei 2011). However, a suitable model for the water inrush mechanism is difficult to develop because of the complexity of geological conditions. Most previous studies were focused on the water inrush from the perspective of rock mechanics. For example, considering the rock damage properties, Valko and Economides (1994) studied the rock fracture process under the action of hydraulic fracturing. Wang and Park (2003) proposed a flow–stress coupling water inrush model based on an elastoplastic theory, in which the water inrush channel was determined only by the permeability evolution caused by rock deformation. Yang et al. (2007) developed a numerical model that involved the coupled effects of flow, stress, and damage. However, these are not appropriate for weathered rock, especially for completely weathered rock and residual soil due to the soil-like behavior. Completely weathered granite has a large amount of fine particles, but little cementation, which makes them prone to disintegration and water erosion. Therefore, it is essential to reconstruct a suitable model for completely weathered granite considering the erosion behavior of particles.

To control water inrush in completely weathered granite, grouting and jet grouting techniques are commonly used methods (Littlejohn 2002a, b; Ni and Cheng 2011, 2014; Shen et al. 2013a, b). The grouting design must be carried out with the consideration of the main factors such as material used, grouting control, and grout parameters. Selection of the grout material is the key to control the groundwater inrushing, which relies on the hydrogeological conditions. The materials are required to satisfy the groutability for permeation grouting so that the grout can be penetrated into the ground. In addition, the special grouts such as polyurethane grouts should be considered in dynamic water grouting, especially for the water inrush disasters (Li et al. 2016). The control of grouting including grouting pressure and grouting spread, is vital to the success of grouting operations. According to a UFC report (2004), high pressure can result in the spread of grout into areas beyond any possible usefulness or damages to structures by displacing the rock. To enable the use of high pressures in order to inject the desired volume of grout while avoiding damages to the rock structure, Lombardi and Deere (1993) proposed a grout intensity number (GIN) method. The concept of this method was to limit the combination of pressure and grouting volume to a specific GIN in order to control the energy induced in the rock fractures and to avoid uplift. However, due to uncertainties in recognizing the distance of grout spread and the state of the fractures, it still has many difficulties in employing this method (Rafi and Stille 2015). The spread of grout was governed by a lot of complex relations, and the understanding was more or less based on empirical knowledge until 1990 (Houlsby 1990). Recently, a new active control method for permeation grouting, called "real time grouting control method", had been developed for governing the grout spread during the grouting operation (Stille et al. 2009, 2012). This method had been applied in the tunnel projects in Sweden successfully, indicating that the method could be applicable to real grouting design and control. Nevertheless, those methods were limited in the grouting design for completely weathered granite because of the groutability as demonstrated in the project of Xiang'an subsea tunnel (Zhang et al. 2014a) and Hong Kong mass transit railway (Bruce and Shirlaw 1985). The grouting process in completely weathered granite is dominated by fracture grouting rather than permeation grouting due to the large amount of fine particles. However, curtain grouting thickness, which is the key parameter for grouting design, must be determined in both fracture grouting and permeation grouting. During recent decades, many studies on the selection of curtain grouting thickness have been conducted with numerical and experimental methods and engineering experience (Carter et al. 2003; Ritchie et al. 2003; Chai and Cui 2012; Zhang et al. 2015). However, these studies all ignored the effects of particle loss, which will lead to an unreasonable curtain grouting for completely weathered granite.

The objective of this paper is to propose a seepage–erosion coupling water inrush model for completely weathered granite by taking into account the migration of particles. This model, which made up for the deficiencies of ignoring the disintegration and erosion features, could be better used to predict the development of water inrush and to simulate the overall response of a medium arising from the erosion process. Then, the proposed water inrush model was applied to numerically examine the influence of curtain grouting thickness on the seepage–erosion process. Moreover, the curtain grouting thickness obtained from the proposed method was applied to Cenxi tunnel in China. The study results showed that the numerical results based on the proposed model agreed well with field tests. The proposed model and the corresponding curtain grouting technology could improve the understanding for water inrush mechanism, ameliorate the design method for curtain grouting, and provide a reference for similar engineering scenarios.

Seepage–erosion water inrush model

Basic assumptions and definitions

Basic assumptions: (1) completely weathered granite is considered a three-phase system consisting of solid grains (sg), fluid (f), and fluidized solids (fs). The fluidized grains are regarded as suspended particles that move with the fluid. (2) The pore spaces are completely filled with fluid and fluidized grains. (3) The velocity of fluidized grains is always equal to the fluid velocity.

Basic definitions: (1) the volume fraction of the α phase is $n^a = \mathrm{d}V^a/\mathrm{d}V$, where the α phase represents the solid grain phase, fluid phase or fluidized grain phase; $\mathrm{d}V^a$ is the volume of the α phase; $\mathrm{d}V$ is the volume element of the three-phase medium. (2) The partial density of the three phases is defined as $\rho^a = \mathrm{d}m^a/\mathrm{d}V$, where $\mathrm{d}m^a$ is the mass of the α phase. (3) The real density of the α phase is $\rho^{\alpha'} = \mathrm{d}m^a/\mathrm{d}V^a$, for which the fluidized grain phase shares the same real density with solid grain phase; $\rho^{sg'} = \rho^{fs'} = \rho^{s'}$, $\rho^{s'}$ is the real density of soil particles, and $\rho^{f'}$ is the real density of the fluid. (4) The porosity φ and the concentration α of the fluidized grains in the fluid are defined as $\varphi = \mathrm{d}V_V/\mathrm{d}V = n^f + n^{fs}$ and $c = \mathrm{d}V_{fs}/\mathrm{d}V_V = n^{fs}/(n^f + n^{fs})$, respectively, where $\mathrm{d}V_V$ is the pore volume.

Governing equations

The seepage–erosion water inrush model uses a set of mass balance equations for constraining the interaction of the three phases, a porosity evolution equation for describing the erosion of fluidized grains, and a coupled Darcy–Brinkman/Navier–Stokes equation for the fluid flow.

Mass balance equations

For a multi-phase flow system, the mass balance equation can be expressed as follows (Bear 1972):

$$\frac{\partial \rho^a}{\partial t} + \mathrm{div}(\rho^a v^{a'}) = \dot{m}^a, \tag{1}$$

where $v^{a'}$ is the real velocity of the α phase, the term $\dot{m}^a$ on the right-hand side of Eq. (1) represents the mass generation rate of the α phase, the first term on the left is the partial density change rate of the α phase, and the second term represents the net accumulation term of the α phase.

According to the Dupuit–Forchheimer law (Bear 1972), the volume discharge q_i of the fluid–particle mixture is related to the velocity v_i as follows:

$$v_i = q_i/\varphi \tag{2}$$

Therefore, the mass balance equations of the three phases are as follows:

$$\text{Solid grains phase:} \frac{\partial \varphi}{\partial t} = \frac{\dot{m}}{\rho_s} \tag{3}$$

$$\text{Fluidized grains phase:} \frac{\partial (c\varphi)}{\partial t} + \nabla(cq_i) = \frac{\dot{m}}{\rho_s} \tag{4}$$

$$\text{Fluid phase:} \nabla q_i = 0, \tag{5}$$

where $\dot{m}$ represents the rate of produced mass (here removed due to erosion).

Equations (3)–(5) constitute a set of three mass balance equations for the three considered phases of completely weathered granite. There are four independent unknown variables φ, c, q_i, and $\dot{m}$; thus, one additional equation is necessary for solving this erosion problem. Therefore, a porosity evolution law is established in "Porosity evolution law".

Porosity evolution law

Extensive theoretical and experimental studies in relation to the mass generation or erosion problem in porous media were run in the late 1990s by many scholars (Vardoulakis et al. 1996; Stavropoulou et al. 1998). These works, summarized in the paper by Rahmati et al. (2013), resulted in many constitutive equations that govern the erosion process. These ideas are adopted to describe the process of piping and sand production in the form of a porosity evolution law for the rate of eroded mass as follows:

$$\frac{\partial \varphi}{\partial t} = \dot{m}/\rho_s = (\dot{m}_{er} - \dot{m}_{dep})/\rho_s = \lambda(1 - \varphi)(c - c^2/c_{cr})|q|, \tag{6}$$

where λ is the coefficient of the porosity evolution equation, $|q|$ is the module of volume discharge q, $\dot{m}_{er}$ is the rate of eroded mass, $\dot{m}_{er} = \rho_s \lambda (1 - \varphi) c |q|$, where $\dot{m}_{dep}$ is the rate of deposited mass, and $\dot{m}_{dep} = \rho_s \lambda (1 - \varphi) |q| c^2 / c_{cr}$, where c_{cr} is a critical value of c for which the two competing phenomena, erosion and deposition, balance each other.

However, water inrush has some differences with piping and sand production because both the fine and coarse particles will be eroded. This leads to a higher concentration c of fluidized grains than piping and sand production. Moreover, the fast fluid velocity will result in a much higher rate of eroded particle mass, greater than the rate of deposited mass for water inrush. Therefore, Eq. (6) will be simplified as follows by ignoring the deposition phenomena.

$$\frac{\partial \varphi}{\partial t} = \lambda (1 - \varphi) c |q| \tag{7}$$

From Eq. (7), the derivation of porosity is proportional to the concentration c. If c is non-zero, the erosion process, modeled by such a law, will run until all of the mass is eroded away, namely the porosity $\varphi = 1$. However, Hu and Ma (2013) and Zhang et al. (2014b) conducted seepage–erosion experiments and showed that the collapse or water inrush occurred before the porosity $\varphi = 1$. A maximum stable porosity was observed in the erosion process, where the seepage–erosion process became stable, mass transfer did not occur and the porosity remained unchanged. Thus, considering the maximum porosity, the porosity evolution Eq. (7) needs to be further modified as follows:

$$\frac{\partial \varphi}{\partial t} = \lambda (\varphi_m - \varphi) c |q|, \tag{8}$$

where φ_m is the maximum porosity of completely weathered granite, which is related to the physical properties of the medium, the particle size distribution and the stress state. Through the study of seepage–erosion coupled experiments and internal soil erosion (Bendahmane et al. 2008; Chang and Zhang 2011), the relationship between maximum porosity and physical and mechanical properties is concluded as follows:

$$1/(\varphi_m - \varphi_0) = a + b/|i|, \tag{9}$$

where φ_0 is the initial porosity, $|i|$ is the module of the hydraulic gradient i, and the parameters α and b can be calculated experimentally, which reflects the influences of the medium physical properties and stress state. The final adoptive porosity evolution equation for water inrush can be expressed as follows:

$$\frac{\partial \varphi}{\partial t} = \lambda [(\varphi_0 + 1/(a + b/|i|)) - \varphi] c |q| \tag{10}$$

Water inrush mechanism and coupled seepage equations

Water inrush in completely weathered granite is a coupled seepage–erosion process. The evolution process of water inrush can be divided into three stages (Zhang et al. 2014b): (1) the initial linear flow stage at the beginning, in which the fluid flow is very slow and the flow is a linear laminar flow; (2) the rapid flow stage, in which the porosity is obviously increased with the loss of particles, thus leading to a rapid increase of flowing velocity; (3) the pipe flow stage which occurs after the formation of the water inrush channel, in which the flow transforms into pipe flow.

To depict the change in the flow pattern in the whole time evolution process of water inrush, a coupled Darcy–Brinkman/Navier–Stokes equation is introduced from the literature (Hill and Carr 2010). The coupled equation for porous media can be expressed as follows:

$$\frac{\bar{\rho}}{\varphi} \left(q_i \cdot \nabla \frac{q_i}{\varphi} \right) = \nabla \cdot (-pI)$$
$$+ \nabla \left\{ \frac{1}{\varphi} \left[\eta_k (\nabla q_i + (\nabla q_i)^T) - \frac{2\eta_k}{3} (\nabla q_i) I \right] \right\} \tag{11}$$
$$- \frac{\eta_k}{k} q_i + F$$
$$\nabla q_i = 0,$$

where p is the pore pressure, η_k is the kinematic viscosity of the fluid, F is the body force term, I is the unit matrix, $\bar{\rho}$ is the partial density of fluid and fluidized grain mixture; $\bar{\rho} = c\rho^{s'} + (1 - c)\rho^{f'}$. k is the permeability of the porous medium. In addition, the permeability can be expressed by the porosity using the Kozeny–Carman formula:

$$k = k_0 \frac{\varphi^3}{(1 - \varphi)^2}, \tag{12}$$

where k_0 is the initial permeability of porous media.

The left term in Eq. (11) is the inertia term of the Navier–Stokes equation. The second term on the right denotes the viscous term of Brinkman's model (Brinkman 1949), and the third term is the viscous term of Darcy's law.

It can be observed from Eq. (11) that the equation can be simplified to Darcy's equation by neglecting the inertia term and the viscous term of Brinkman's equation when the flow velocity is very small. As the evolution process enters into the rapid flow stage, it has the advantage of approximating brinkman's equation which is more suitable for the fast-moving fluid in high porosity medium. When the channel has formed, the inertia term of Navier–Stokes will obviously increase, and the equation can be approximate to Navier–Stokes equation to describe the third stage.

The basic unknowns in the coupled seepage–erosion water inrush Eqs. (3)–(5), (10)–(12) are only p, c, and φ. Combining the relative initial conditions and boundary

conditions, these PDE equations can be solved numerically by adopting the Galerkin finite method and implicit difference method to discretize space and time. Considering the non-linearity of the equation system, the solution can be obtained with the Newtown–Raphson iteration method. With these methods, the "*COMSOL* Multiphysics system" was adopted to solve these PDE equations by secondary development in this paper.

Numerical simulation of water inrush behavior considering the effect of curtain grouting thickness

Brief introduction to the Cenxi highway tunnel

Cenxi highway tunnel, 4288 m in length, is located on the highway from Cenxi city to Shuiwen city in Guangxi Province, China. Because of complex geological conditions and serious water inrush disasters, the tunnel was the key engineering challenge of the highway.

Geological conditions

The tunnel is located in a valley with a V shape, and the buried depth of the tunnel is approximately 96 m. The area from CK7 + 838.5 to CK7 + 981.6 is the unexcavated part at present. There is a large completely weathered granite region with abundant water in the tunnel. The water pressure is approximately 0.7–1 MPa, and the rock quality designation (RQD) of the surrounding rock of the residual tunnel was less than 5%. The geological prospecting was assessed based on the vertical and horizontal borehole information (see Fig. 1). A geological profile of the tunnel is given in Fig. 2. It can be concluded from Figs. 1 and 2 that the lithology of the residual tunnel was mainly completely weathered granite.

Water inrush disasters

Because of these complex geological conditions, from September 11, 2013 to October 23, 2015, four large-scale water and mud inrush incidents occurred in Cenxi tunnel, and the volume of gushing water and mud was greater than 250,000 m^3 in total (Fig. 3). Great economic loss and secondary disasters were caused by these geological events, which seriously hindered the construction.

To overcome these difficult geological conditions, the whole-section curtain grouting was adopted. Numerical simulation and field tests were conducted to determine the scheme of the curtain grouting. First, the new water inrush model mentioned above was used to determine the curtain grouting thickness by numerical simulation, and the final

(a) Vertical boreholes of Sk4 (0-108.76m)

(b) Horizontal boreholes of CK7+950—CK7+945

Fig. 1 Lithology of vertical and horizontal boreholes

decision was made based on field investigations of the grouting effect.

Numerical model and boundary conditions

Based on the geological conditions of Cenxi tunnel, a simplified circular tunnel has been built to study the curtain grouting thickness, as illustrated in Fig. 4, in which the tunnel radius r_a is 7.5 m, the external radius of the reinforcement cycle is r_b, and the curtain grouting thickness is r. The exterior of the curtain grouting is assumed to be a water-rich zone with water pressure p_b, and the internal pressure of the tunnel excavation contour line (free surface)
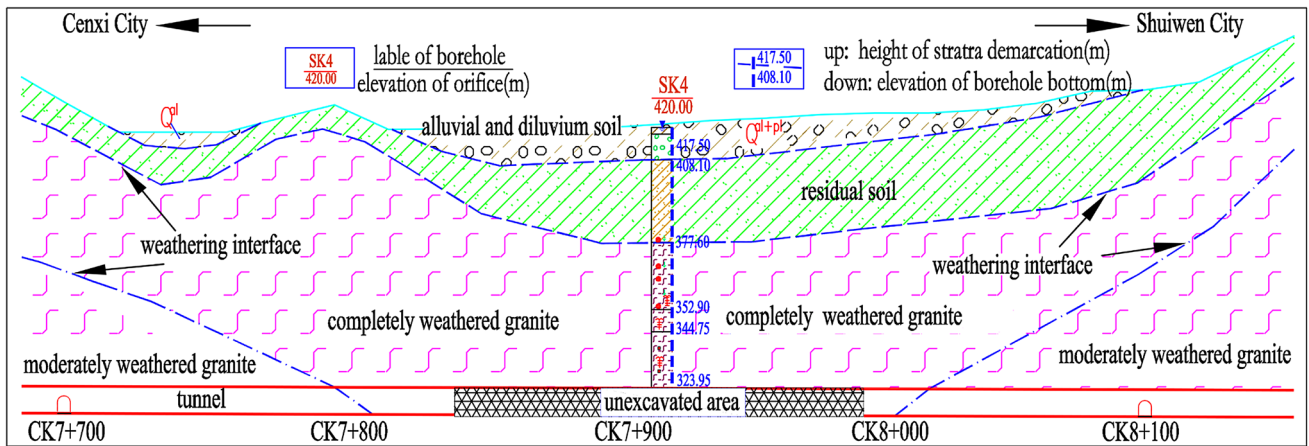
Fig. 2 Geological profile of unexcavated area

(a) Water inrush

(b) Mud inrush

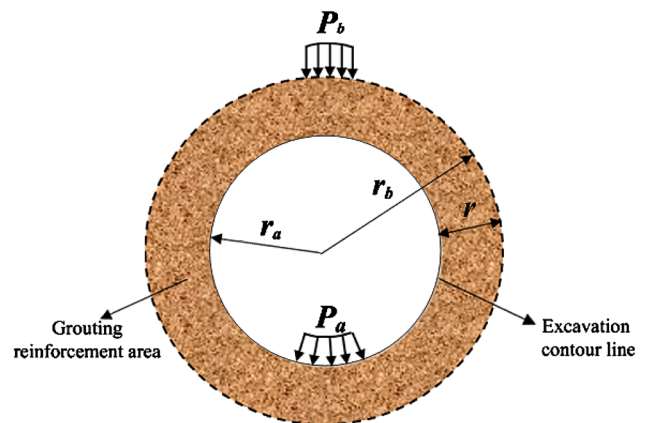**Fig. 3** Large-scale water and mud inrush

Fig. 4 Scheme of calculation model

is assumed to be p_a. The fluid flow is considered to be radial (towards the excavation contour line).

The physical parameters of the numerical simulation are shown in Table 1. The permeability value K_i after grouting was tested under the condition of 80% grouting filling ratio (GFR), which indicates the volume ratio of grouting quantity and initial stratum porosity. The initial porosity φ_i after grouting was decided by theoretical calculation by means of completely filling the porosity with grouting, namely, $\varphi_i = (1 - GFR) \times \varphi_0$.

The initial porosity and fluidized grain concentration in the reinforcement cycle are φ_i and c_i, respectively. The initial pore pressure in the whole region was obtained from the initial steady seepage calculation. The outside boundary r_b was set for a water-rich zone with water pressure $p(r_b, t) = 1$ MPa, porosity $\varphi(r_b, t) = \varphi_i = 0.072$, and fluidized grain concentration $c(r_b, t) = c_i = 0.01$. The internal boundary r_a was set for a free surface on which particles can freely migrate with water, and the water pressure $p(r_a, t) = 0$ MPa.

Table 1 Physical parameters of the numerical simulation

Parameters	Value
Partial density of fluid $\rho^{f'}$	1000 kg/m³
Partial density of grains $\rho^{s'}$	2650 kg/m³
Kinematic viscosity of the fluid η_k	1×10^{-6} m²/s
Initial permeability of surrounding rock before grouting K_0	4×10^{-12} m²
Initial permeability of surrounding rock after grouting K_i	1.2×10^{-14} m²
Initial porosity of surrounding rock before grouting φ_0	0.36
Initial porosity of surrounding rock after grouting φ_i	0.072
Frequency λ	5 m⁻¹
Parameter a	1.533
Parameter b	153.4
Initial concentration of fluidized grains c_i	0.01
External pore pressure P_a	1 MPa
Internal pore pressure P_0	0 MPa
Curtain grouting thickness r	2–8 m

Numerical results and analysis

The seepage–erosion process is discussed, and the results are presented in two sets of plots. The first set of Figs. 5, 6, 7 and 8 depicts the spatial profiles of the various properties for different curtain grouting thicknesses at the given time ($t = 12$ h).

Figure 5 is the porosity contours of various curtain grouting thicknesses at $t = 12$ h. Figure 5a shows that the porosity of whole region is high at 0.7 when the curtain grouting thickness is only 2 m, which actually indicates that collapse or water inrush has occurred. Even when the curtain grouting thickness increases to 4 m, it is still at great risk of a water inrush disaster because the porosity has evidently increased, especially at a distance of 2 m from the excavation contour line.

When the curtain grouting thickness increases to 6 m, the increase in porosity and the affected area decrease rapidly, and the maximum porosity is only 0.13. Furthermore, the porosity continues to decrease, but mainly remains constant when the thickness exceeds 6 m as shown in Fig. 5f, g. Combining Fig. 6, it can be observed that the porosity increases significantly in the whole curtain area when the curtain grouting thickness is less than 6 m, and the seepage–erosion process is suppressed when the thickness exceeds 6 m, which results in a very small change in porosity in the reinforcement area.

For the lower curtain grouting thickness (less than 6 m), this porosity distribution results in the permeability distribution shown in Fig. 7 according to the Kozeny–Carman Eq. (12), which reflects the significant permeability inhomogeneity evolution as a result of the seepage–erosion process. This permeability inhomogeneity evolution leads to a nonlinear pore pressure distribution with obviously lower pressure gradients in the seepage–erosion region (Fig. 8). With increasing curtain grouting thickness, the permeability maintains a homogeneous distribution with little change, and the pore pressure maintains an approximately linear distribution along the distance, which indicates a weaker erosion effect.

In the second set of Figs. 9 and 10, the time evolution of the various properties of different curtain grouting are shown at the excavation contour line, which is of interest. Figure 9 shows the effect of the curtain grouting thickness on the particle mass transfer. As the thickness increases, the erosion effect decreases and the lower particle mass is lost, as is demonstrated in Fig. 9a. It is apparent that most of the region has suffered significant mass transfer when the thickness is less than 6 m. The slope of these curves is the rate of particle loss mass (Fig. 9b), and showing that the rate increases as time initially and gradually decreases to a lower value for the lower thickness.

Figure 10a shows the regulation of transport concentration c of fluidized grains versus time. The value of concentration c consists of the convection and mass generation, and the increase in concentration with time indicates that the erosion process remains more active than the transport process until the point at which the convection overtakes the mass generation. This indicates that the erosion process has almost been completed, and the water inrush channel has been formed when the transport concentration tends to decreasing, which is demonstrated in Fig. 10a.

Mass transfer naturally leads to porosity evolution, as shown in Fig. 10b. Figure 10b shows that the porosity increases sub-linearly with time. Such a porosity evolution law results in the same law of permeability according to Eq. (12), as shown in Fig. 10c. A significant increase in

Fig. 5 Spatial contours of
porosity at various curtain
grouting thickness at $t = 12$ h

(a) r=2m

(b) r=3m

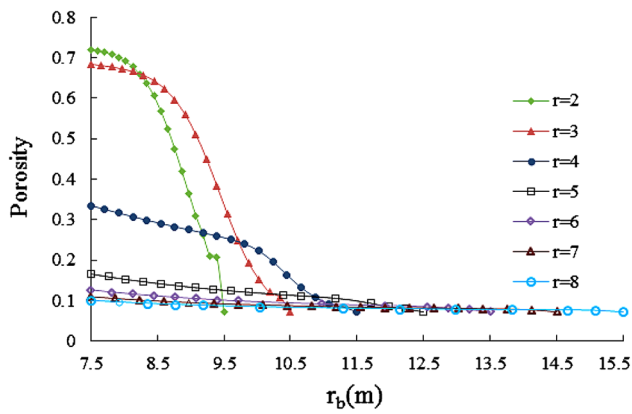(c) r=4m

(d) r=5m

(e) r=6m

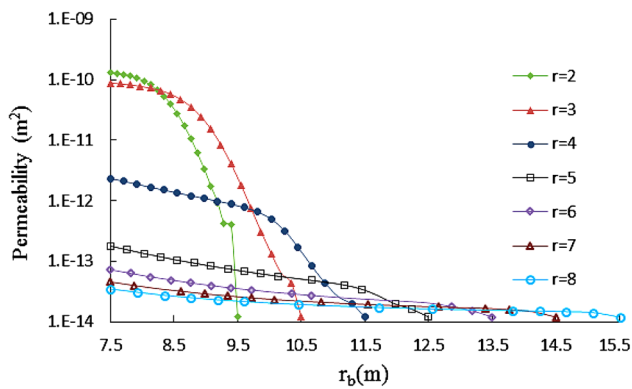(f) r=7m

(g) r=8m
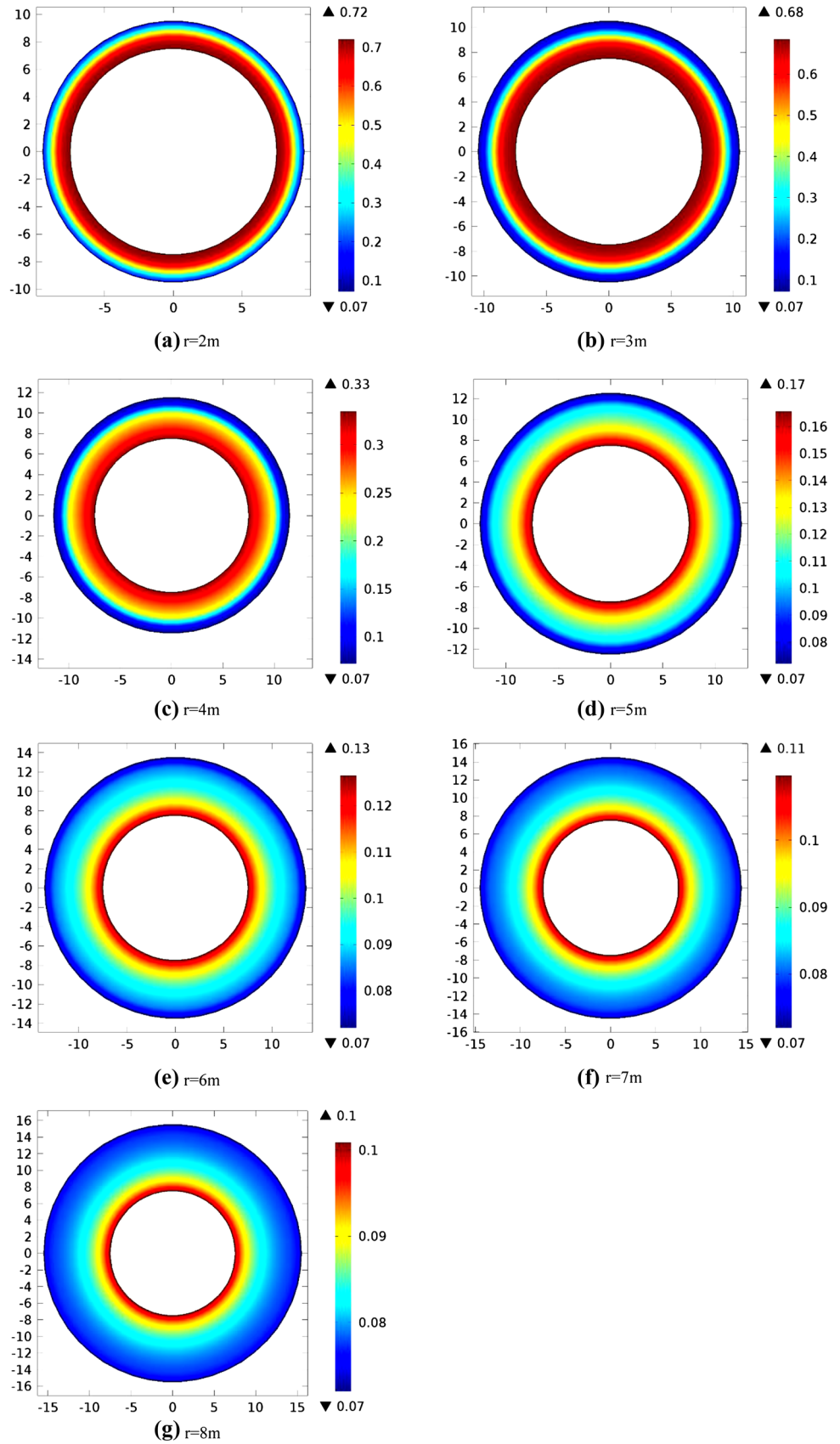
Fig. 6 Spatial profile of porosity at $t = 12$ h

Fig. 7 Spatial profile of permeability at $t = 12$ h
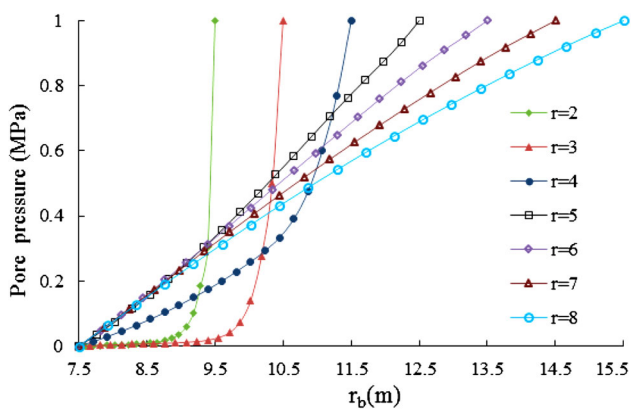
Fig. 8 Spatial profile of pore pressure at $t = 12$ h
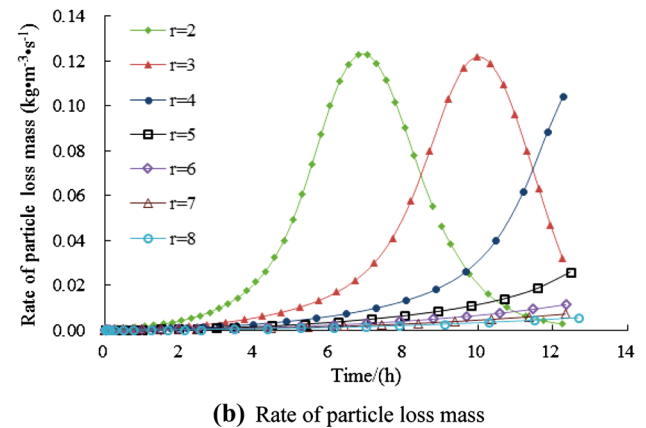

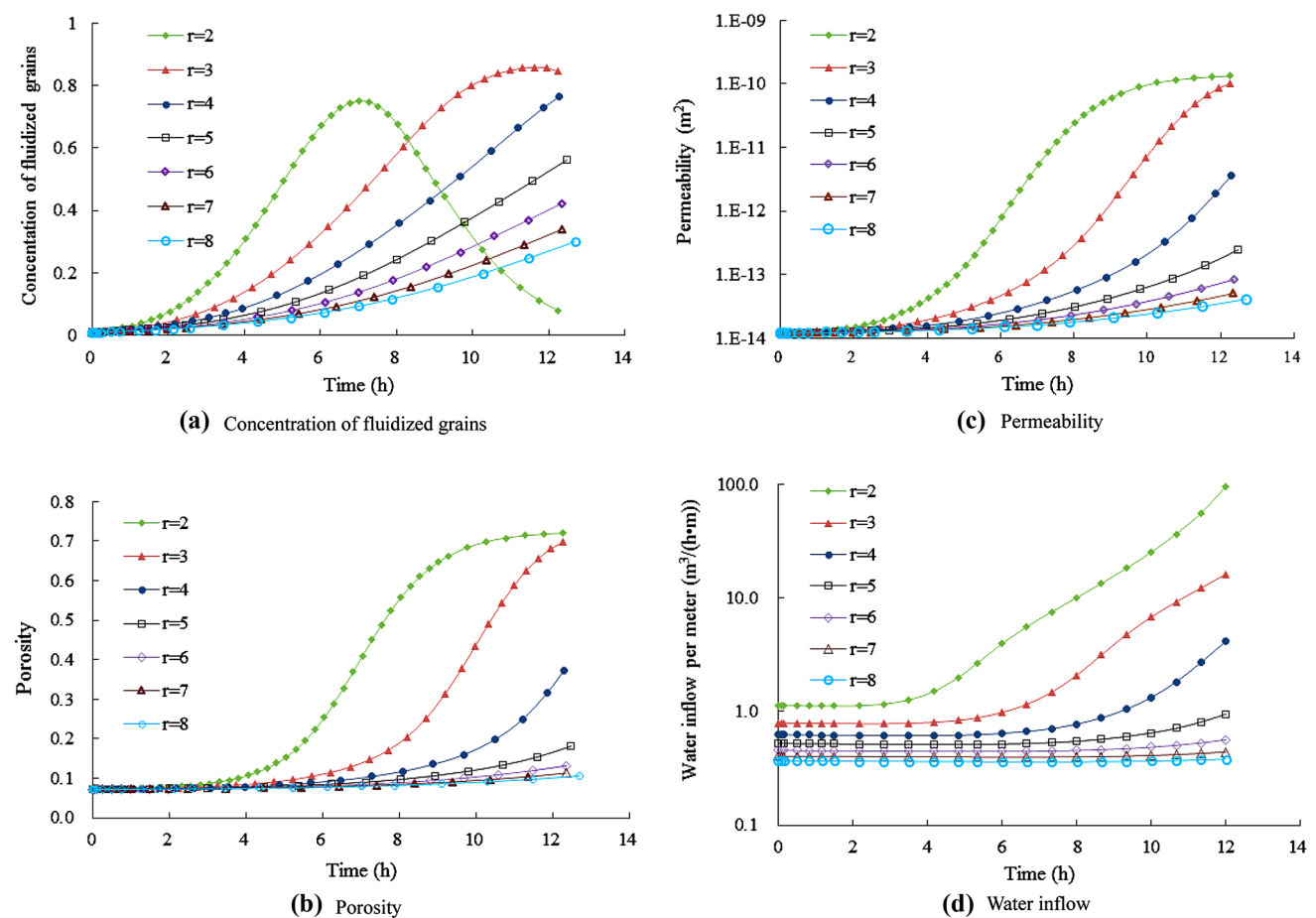(a) Particle loss mass

(b) Rate of particle loss mass

Fig. 9 Time evolution of mass transfer characters at the excavation contour line of the tunnel

thickness less than 6 m, and the water inflow diminished rapidly with thickness increasing. The water inflow for the thickness of 2–8 m are 96.8, 16.3, 4.2, 0.95, 0.56, 0.44, 0.38 m^3/h. The values for the thickness of less than 6 m greatly exceed the acceptable criterion 0.6 m^3/h (10 L/min) (Wang et al. 2011), which is the widely used to determine the condition of tunnel excavation in engineering.

Based on the above analysis, it can be concluded that the thickness of 6 m is the appropriate parameter of curtain grouting in completely weathered granite.

Field investigation of hydraulic and mechanical behavior of curtain grouting

To verify the effectiveness of the developed water inrush model and the thickness of curtain grouting proposed above, a field test of curtain grouting was carried out in Cenxi tunnel. The hydraulic and mechanical behavior of curtain grouting that reflected the grouting reinforcement effect was examined by examination holes, P–Q–t curve, geophysics prospecting, and excavation.

porosity raises the permeability by a factor of more than 300 times when the thickness is lower than 6 m. However, the increase in the other thickness is by a factor of no more than ten times. In addition, the development of water inflow will be accelerated with increasing permeability according to the seepage equation as shown in Fig. 10d. From Fig. 10d, it is obvious that the water inflow with thickness greater than 6 m is much smaller than that with

(a) Concentration of fluidized grains

(c) Permeability

(b) Porosity

(d) Water inflow

Fig. 10 Time evolution of key parameters at the excavation contour line of the tunnel

Brief introduction of the curtain grouting design in Cenxi tunnel

The key parameters of curtain grouting were designed as follows.

1. According to the results of the numerical simulation, an effective curtain grouting thickness of 6 m was adopted. The grouting reinforced length was 25 m, and the terminal distance between the grouting holes and the diffusion radium of the grouting was designed to be 2.8 and 2 m, respectively.
2. Ninety-five grouting holes including seven cycles from outside to inside were designed in total, and the construction sequence of grouting was carried out from the cycle A holes to the cycle G holes (see Figs. 11, 12). The terminal grouting pressure of the design was 4–6 MPa.
3. The composite grouting materials were adopted to treat different hydraulic conditions including the cement grout, cement-sodium silicate grout and cement-GT grout, which had different advantages in terms of strength, anti-wash, or gel time property (Li et al. 2016; Zhang et al. 2015).

### Hydraulic behavior of examination holes

Seven examination holes were designed to evaluate the grouting reinforcement effect, as shown in Fig. 13. The detailed information, including lithology, hole-making rate and water inflow exposed by examination holes, is shown in Table 3.

Note that the lithology exposed by the examination holes was mainly a mixed solidification body of slurry and completely weathered granite for the first 20 m. The last few meters (approximately 5 m) mainly comprised completely weathered granite with a small amount of slurry particles and high sand content (see Table 2; Fig. 14), and the rates of coring are high at 60%. This result indicated that the unfavorable geology area was reinforced effectively, especially for the first 20 m. In addition, all hole-making rates exceeded 70%, which showed that there was no obvious collapse in the examination holes and further showed that the surrounding rock had good steadiness. Furthermore, the water inflows, the most critical factor of the grouting effect indicating the water plugging performance for completely weathered granite, were 0.013, 0.019, 0.009, 0.006, 0.100, 0.145, 0.020 L/(min m) for J-1

Fig. 11 Design of curtain grouting
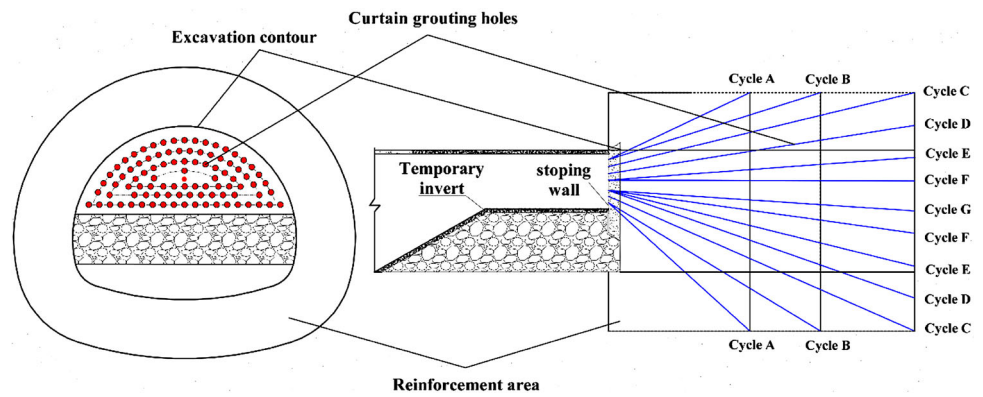
Fig. 12 Construction of curtain grouting
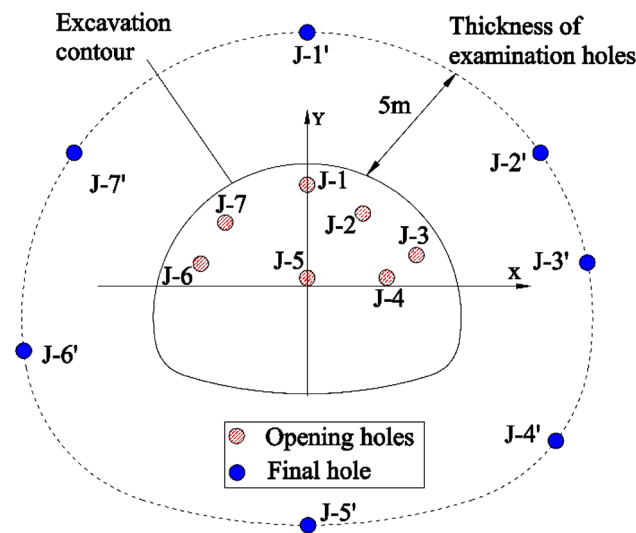
Fig. 13 Layout of opening and final holes for examination holes

to J-7, which were all less than the standard for a single hole per meter (0.2 L/(min m)) in similar engineering (Wang et al. 2011), indicating that the surrounding rock after grouting had good water plugging performance. In

other words, the thickness of the curtain grouting designed by numerical simulation was suitable.

$P–Q–t$ curve of examination holes

Injection pressure (P) and velocity (Q), which can reflect the diffusion characteristics of the grout, the geosphere integrity and compactness, were recorded during the grouting of the examination holes. Because of the similar results for the examination holes, only the $P–Q–t$ curve of hole J-1 was shown in Fig. 15.

For the whole process of grouting, completely weathered granite was reinforced by the filling, permeating, compaction, and splitting effects of the injected grout. Initially, owing to the loose, high porosity, or even void spaces of the geology, the injected pressure was relatively low and the grout played a filling, permeating, and compaction role. At this stage, a large amount of grout was needed to fill and reinforce the surrounding rock and naturally the injection velocity was relatively high. However, when the porosity or void space was completely filled, the grout mainly played a compaction role, and the injected pressure started to increase to overcome the initial minimum principal stress of the medium (Zhang et al. 2014a, 2015). As the pressure increased to overcome the initial stress, the medium was split by grout with the formation of a large space. Thus, the injection pressure decreased rapidly and the injection velocity increased rapidly.

After the completion of curtain grouting, the compactness and strength of the medium was expected to be greatly improved. Furthermore, when carried out the test of $P–Q–t$ curve in the examination holes, the injection pressure was expected to increase rapidly to exceed the designed terminal pressure and the injection velocity was expected to decrease rapidly (as in Fig. 15). Conversely, if the injection pressure was still very low and the injection velocity was very high for a long time, indicating that the medium still has significant weak areas.

Table 2 Results of examination holes

Label	Lithology	Hole-making rate (%)	Water inflow (L/min m)
J-1	0–6 m: solidification body of slurry	93.8	0.013
	7–18 m: mixed solidification body of slurry and completely weathered granite without water		
	19–26 m: completely weathered granite with a small amount of slurry particle and high sand content		
J-2	0–6 m: solidification body of slurry	100.0	0.019
	7–16 m: mixed solidification body of slurry, gravel and completely weathered granite without water		
	17–26 m: completely weathered granite with a small amount of slurry particle and high sand content		
J-3	0–6 m: solidification body of slurry	100.0	0.009
	7–18 m: mixed solidification body of slurry, gravel and completely weathered granite without water		
	19–25 m: completely weathered granite with a small amount of slurry particle and high sand content		
J-4	0–6 m: solidification body of slurry	88.2	0.006
	7–21 m: mixed solidification body of slurry, gravel and completely weathered granite without water		
	22–27 m: completely weathered granite with a small amount of slurry particle and high sand content		
J-5	0–6 m: solidification body of slurry	75.4	0.100
	7–21 m: mixed solidification body of slurry, gravel and completely weathered granite without water		
	22–28 m: completely weathered granite with a small amount of slurry particle and high sand content		
J-6	0–6 m: solidification body of slurry	78.9	0.145
	7–20 m: mixed solidification body of slurry, gravel and completely weathered granite without water		
	21–27 m: completely weathered granite with a small amount of slurry particle and high sand content		
J-7	0–6 m: solidification body of slurry	93.8	0.020
	7–16 m: mixed solidification body of slurry, gravel and completely weathered granite without water		
	17–26 m: completely weathered granite with a small amount of slurry particle and high sand content		

Figure 15 showed that the injection pressure rapidly increased to 6.8 MPa, and the injection velocity sharply decreased to 8 L/min in 6 min, which satisfied the design qualification of injection pressure and velocity, indicating that the unfavorable geology was reinforced by the grouting.

Geophysical prospecting by the transient electromagnetic method

Before tunnel excavation, it is critically important to understand the geological conditions in front of the tunnel face. In tunnel construction, geophysical prospecting is a common and useful advanced forecast geology method. The transient electromagnetic (TEM) method, is a geophysical prospecting methods in which electric and magnetic fields are induced by transient pulses of electric current and the subsequent decay response measured. The resistivity (or conductivity) distribution in the ground, which is directly related to the geotechnical characteristic, can be effectively measured by observing the currents diffuse in the subsurface (McNeill 1994). TEM is the most sensitive method to distinguish low resistivity geological bodies such as water-bearing structure in high resistivity surrounding rock. This is the reason why this method had been developed rapidly in recent years and made great

progress at hydrogeophysic survey and groundwater exploration fields (Danielsen et al. 2003; Christiansen et al. 2009). Therefore, this method was used to analyze the grouting reinforcement effect in Cenxi tunnel by comparison of pre- and post-grouting, as shown in Fig. 16. It can be seen from the left of Fig. 16 that there is an obvious low-resistivity region on the right side of the tunnel face before grouting. Moreover, the distance between the low-resistivity region and the tunnel face is approximately 10 m, especially behind the distance of 18 m, indicating that there may be a water-rich body. This assumption was confirmed by the subsequent exposure of water-rich geology by drilled holes. After grouting, the resistivity from the tunnel face to the forth distance of 30 m was significantly improved, as shown on the right side of Fig. 16, which shows that the water has been extruded to that distance. Consequently, the region from 10–30 m has been replaced by the grout, indicating that the thickness of curtain grouting of 6 m can be adopted.

Mechanical behavior of curtain grouting

As shown in Fig. 17, the medium is tightly combined with consolidation body of the grout. There are many grout veins in the tunnel face with maximum length of 3.5 m and width of 0.5 m. Some basic physical and mechanical
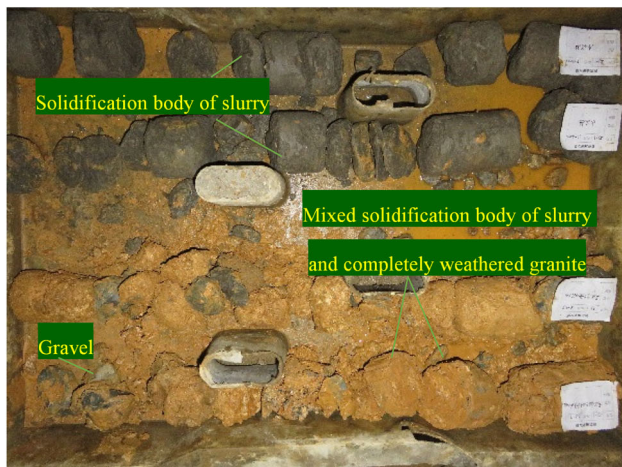
(a) Mixed solidification body of slurry and completely weathered granite

(b) Completely weathered granite with high sand content

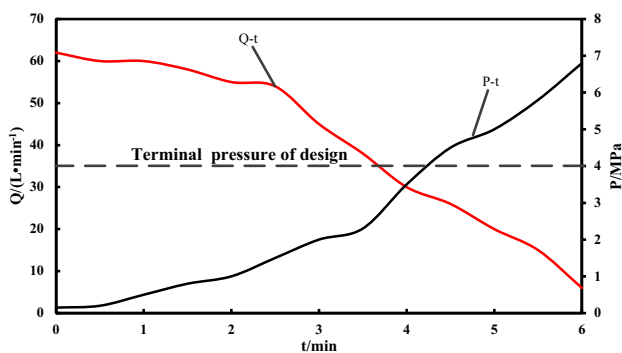**Fig. 14** Lithology exposed by coring of examination holes

Fig. 15 *P–Q–t* curve of J-1 hole

parameters of the medium are tested in the laboratory as shown in Table 3. Table 3 shows that the water content decreased from 22 to 8% after grouting, and the strength obviously increased, indicating the reliability of grouting thickness of 6 m.
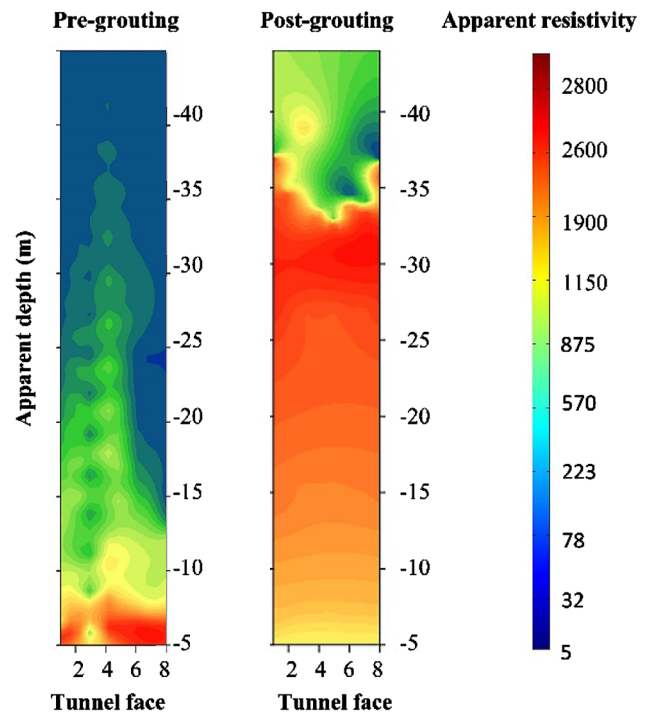

Fig. 16 Transient electromagnetic results pre- and post-grouting
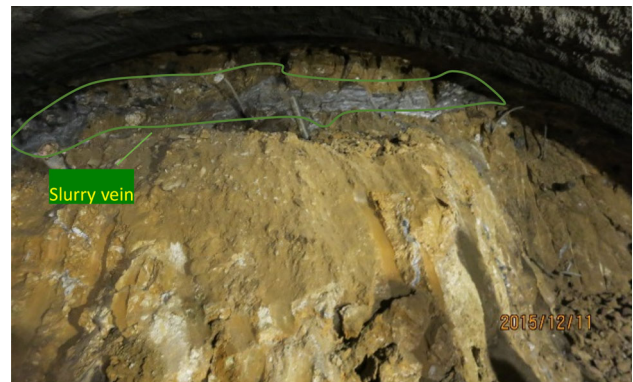

Fig. 17 Grouting effect exposed by excavation

Based on foregoing examinations of the grouting reinforcement effect, it can be concluded that the unfavorable geology has been reinforced well by curtain grouting, and the thickness of 6 m is suitable for the geological conditions of this tunnel.

Discussion

In this paper, we have shown the seepage–erosion behavior in the development of water inrush and their impact on curtain grouting thickness for completely weathered granite. The numerical simulation and field tests indicate that the proposed model and the recommended curtain grouting

Table 3 Physical and mechanical parameters of the reinforced body

Label	Water content	Point load strength	Uniaxial compressive strength	Tensile strength
Cement paste	–	1.8	35.93	1.72
Chemical grout paste	–	0.08	1.63	0.08
Solidification body of slurry and rock	8%	0.46	9.18	0.44
Original rock	22%	Soft-plastic soil with very low strength		

thickness are reliable. It has been confirmed that the particle loss caused by seepage–erosion is a key factor of water inrush in a completely weathered granite tunnel, which should be considered in the design of curtain grouting.

To illustrate the superiority of the method proposed in this paper, the proposed method is compared with the traditional analytical solution and numerical solution based on fluid–structure interaction theory. The analytical solution for water inflow based on steady-state water inflow into a circular tunnel is one of the most widely used method for water inflow prediction and curtain grouting design (Yang et al. 2016; Wu et al. 2015b; Xu et al. 2016). The water inflow Q, depending on the parameters of surrounding rock, lining, and grouting cycle, can be expressed as (Yang et al. 2016):

$$Q = \frac{2\pi H k_r}{\ln(r_2/r_g) + k_r/k_g \ln(r_g/r_1) + k_r/k_1 \ln(r_1/r_o)}, \quad (13)$$

where Q represents the flow through the tunnel; r_o, r_1, r_g are the radius of tunnel, lining, and grouting circle, respectively; r_2 is the depth of the tunnel center from the ground surface. H is the groundwater head above tunnel. k_r, k_g, k_1 are the permeability coefficient of surrounding rock, grouting cycle, and lining, respectively.

Without considering the lining structure, Eq. (13) can be simplified to:

$$Q = \frac{2\pi H k_r}{\ln(r_2/r_g) + k_r/k_g \ln(r_g/r_0)} \quad (14)$$

Therefore, the tunnel water inflow considering the curtain grouting thickness can be obtained from Eq. (14).

Another commonly used method is the numerical simulation based on fluid–structure interaction theory. Zhang et al. (2015) has studied the effects of permeability variation coefficient N (k_r/k_g) and curtain grouting thickness on water inflow by this method.

Now the analytical solution of Eq. (14), numerical solution based on fluid–structure interaction theory (Zhang et al. 2015) and the seepage–erosion method presented in this paper are considered to be the "analytical solution", the "numerical solution", and the "proposed method", respectively. In order to evaluate the grouting effect, the water inflow is adopted as the performance evaluation
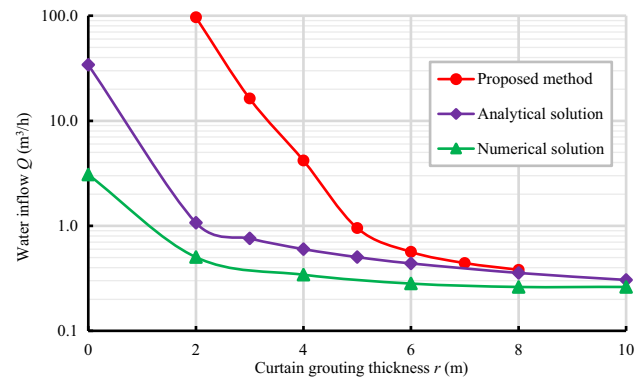
Fig. 18 Comparison of water inflow results for the selected curtain grouting thickness

index. The water inflow is thus calculated based on the model parameters in this paper by using the above three methods. Consequently, the calculated results are illustrated in the Fig. 18.

The comparison results indicate that the water inflows of all selected study curtain grouting thicknesses obtained from the proposed method are larger than the analytical solution and the numerical solution. For example, the water inflow obtained from the proposed method, the analytical solution and the numerical solution is 4.19, 0.60, 0.34 m^3/h, respectively, when the thickness is equal to 4 m. This indicates that the grouting effect evaluated by the previous methods seems much better than the proposed method, and the proposed method seems to decrease the level of grouting effect and increase the risk of water inrush. It may be helpful to understand the results when considering the acceptance criteria of water inflow (<0.6 m^3/h). All the water inflows obtained from the proposed method have exceeded the criteria until the thickness reaches 6 m. However, as long as the thickness is smaller than 4 m, the water inflow obtained from the analytical solution will be greater than the criteria. In addition, it seems to be more effective for the numerical solution because the water inflows all satisfy the criteria unless the curtain grouting is not carried out. This indicates that the design or construction adopting the traditional method such as analytical solution or numerical solution will be more effective than the proposed method, which may be possible in some situations such as in the hard rock or slightly weathered rock.

However, in other situations such as completely weathered granite, the statement that the proposed method decreases the level of grouting effect and increases the risk of water inrush is no longer accurate. For example, the field tests of previous projects such as Xiang'an subsea tunnel (Zhang, et al. 2014a) and Cenxi highway tunnel (in this paper) have demonstrated that the completely weathered granite or strong weathered granite needs to be significantly strengthened. It is necessary to enlarge curtain grouting thickness to increase the level of grouting effect and decrease the risk of water inrush. At last, both of the projects chose a thickness of 6 m. Therefore, this proposed method did not decrease the grouting effect but did increase the grouting effect, thus creating a more scientific and rational curtain grouting design because the proposed method has both considered the seepage and erosion behaviors. However, the previous two methods only consider the seepage behavior or seepage and mechanism behavior, and ignore the vital erosion behavior, leading to the limit of permeability development and water inflow channels.

In addition, Fig. 18 shows that there is a wide gap of water inflow among the three methods, and the gap has widened with the increase of thickness. For example, the water inflow obtained from the proposed method, analytical solution and numerical solution is 0.56, 0.44, and 0.28 m^3/h, respectively, when the thickness is equal to 6 m. The ratio of water inflow for the three methods is 2.0:1.6:1.0. However, the ratio for the three methods has increased to 193.6:2.1:1.0 as the thickness decreases to 2 m. This is because the hydraulic gradient will be significantly increased with the decrease of thickness, resulting in more serious erosion. Moreover, in contrast with the Darcy flow applied in traditional methods, the proposed method use the coupled Darcy–Brinkman/Navier–Stokes equation to describe the fluid flow, which is more effective and accurate to respect the dynamic evolution and seepage mutation of nonlinear flow in the study of water inrush. This indicates that there is a great risk of water inrush without considering the erosion behavior when the thickness is relative small. But when the thickness is large enough, the gap among the three methods seems to be very small so that the erosion behavior can be ignored. However, it is quite difficult to evaluate whether the erosion behavior can be ignored. In other words, the thickness obtained from traditional methods will not be appropriate for completely weathered granite.

However, it should be noted that the mechanical behavior is also an important factor for the water inrush in completely weathered granite. The current study does not adequately consider the mechanical coupling effect. For example, the erosion and the particles loss will eventually change the shear strength and stress status, and then induce rock deformation or even collapse. It is hoped that a modified seepage–erosion–stress coupling will be proposed in the further studies.

Conclusions

1. Considering that particle loss is a key factor of water inrush in a completely weathered granite tunnel, a new seepage–erosion coupled water inrush model is proposed based on theories of solute transport and fluid dynamics in porous media. The new model reflects the dynamics of particle loss, porosity, permeability, pore pressure, and the water inflow induced by the mass transfer of particles, which are factors directly related to the development of water inrush.

2. Using the new water inrush model, the curtain grouting thickness was studied numerically based on practical engineering. The results showed that the seepage–erosion process was aggravated as the thickness increased. When the thickness was less than 6 m, the porosity and permeability visibly changed, and the water inflow clearly exceeded the acceptable engineering criterion. However, with a further increase in thickness, the seepage–erosion process was suppressed and the little changes of the relative parameters were showed.

3. According to the results of a numerical simulation, a thickness of 6 m was selected as an optimal parameter for curtain grouting. This value was shown to be effective, reliable and appropriate after field tests in Cenxi tunnel by means of examination holes, geophysical prospecting, P–Q–t curve, and excavation, and, to a certain extent, can be used as a reference for similar engineering problems.

References

Anno (1995) The description and classification of weathered rocks for engineering purposes. Q J Eng Geol 28:207–242

Arıkan F, Ulusay R, Aydın N (2007) Characterization of weathered acidic volcanic rocks and a weathering classification based on a rating system. Bull Eng Geol Environ 66(4):415–430

Bear J (1972) Dynamics of fluids in porous media. American Elsevier, New York

Bendahmane F, Marot D, Alexis A (2008) Experimental parametric study of suffusion and backward erosion. J Geotech Geoenviron Eng 134:57–67

Brinkman HC (1949) A calculation of the viscous force exerted by a flowing fluid on a dense swarm of particles. Appl Sci Res 1:27–34

Bruce DA, Shirlaw JN (1985). Grouting of completely weathered granite with special reference to the construction of the Hong Kong Mass Transit Railway. In: Proceedings of the 4th international symposium on tunnelling, Brighton, UK, pp 253–264

Carter TG, Amaya F, Jefferies MG, Eldridge TL (2003) Curtain grouting for the Antamina Dam, Peru: part 1—design and performance. In: Grouting and ground treatment. ASCE, pp 917–928

Chai J, Cui W (2012) Optimum thickness of curtain grouting on dam foundation with minimum seepage pressure resultant. Struct Multidiscip Optim 45(2):303–308

Chang DS, Zhang LM (2011) A stress-controlled erosion apparatus for studying internal erosion in soils. Geotech Test J 34:579–589

Christiansen AV, Auken E, Sørensen K (2009) The transient electromagnetic method. In: Groundwater geophysics. Springer, Berlin, Heidelberg, pp 179–226

Cui QL, Wu HN, Shen SL, Yin ZY, Horpibulsuk S (2016) Protection of neighbour buildings due to construction of shield tunnel in mixed ground with sand over weathered granite. Environ Earth Sci 75(6):1–11

Danielsen JE, Auken E, Jørgensen F, Søndergaard V, Sørensen K (2003) The application of the transient electromagnetic method in hydrogeophysical surveys. J Appl Geophys 53(4):181–198

Font-Capó J, Vázquez-Suñé E, Carrera J, Martí D, Carbonell R, Pérez-Estaun A (2011) Groundwater inflow prediction in urban tunneling with a tunnel boring machine (TBM). Eng Geol 121(1):46–54

Gamon TI (1986) Discussion on 'Completely weathered granite—soil or rock?' by MD Howat. Q J Eng Geol Hydrogeol 19(4):433–437

Hill AA, Carr M (2010) Nonlinear stability of the one-domain approach to modelling convection in superposed fluid and porous layers. In: Proceedings of the Royal Society of London A: mathematical, physical and engineering sciences. The Royal Society, p rspa20100014

Houlsby AC (1990) Construction and design of cement grouting: a guide to grouting in rock foundations, vol 67. Wiley, New York

Howat MD (1985) Completely weathered granite—soil or rock? Q J Eng Geol Hydrogeol 18(3):199–206

Hu YY, Ma P (2013) Mechanism study and finite element simulation of three-phase coupling seepage erosion piping. Rock Soil Mech 34:913–921 **(in Chinese)**

Irfan TY (1997) Mineralogical and fabric characterization and classification of weathered volcanic rocks in Hong Kong Special Project Report SPR 1/97. Geotechnical Engineering Office, Hong Kong Government

Li SC, Liu RT, Zhang QS, Zhang X (2016) Protection against water or mud inrush in tunnels by grouting: a review. J Rock Mech Geotech Eng 8(5):753–766

Littlejohn S (2002a) The development of practice in permeation and compensation grouting: a historical review (1802–2002): part 1 permeation grouting. In: Grouting and ground treatment. ASCE, pp 50–99

Littlejohn S (2002b) The development of practice in permeation and compensation grouting: a historical review (1802–2002): part 2 compensation grouting. In: Grouting and ground treatment. ASCE, pp 100–144

Liu XX, Xu YS, Cheng WC, Shen SL (2016) Investigation of hydraulic parameters of a weathered mylonite fault from field pumping tests: a case study. Bull Eng Geol Environ. doi:10. 1007/s10064-016-0910-6

Lombardi G, Deere D (1993) Grouting design and control using the GIN principle. Int water Power Dam Construct 45(6):15–22

McNeill JD (1994) Principles and application of time domain electromagnetic techniques for resistivity sounding. Geonics, technical note TN-27

Ni JC, Cheng WC (2011) Shield machine disassembly in grouted soils outside the ventilation shaft: a case history in Taipei Rapid Transit System (TRTS). Tunn Undergr Sp Technol 26(2):435–443

Ni JC, Cheng WC (2012) Steering characteristics of microtunnelling in various deposits. Tunn Undergr Sp Technol 28:321–330

Ni JC, Cheng WC (2014) Quality control of double fluid jet grouting below groundwater table: case history. Soils Found 54(6):1039–1053

Rafi JY, Stille H (2015) Applicability of using GIN method, by considering theoretical approach of grouting design. Geotech Geol Eng 33(6):1431–1448

Rahmati H, Jafarpour M, Azadbakht S, Nouri A, Vaziri H, Chan D, Xiao Y (2013) Review of sand production prediction models. J Pet Eng 2013:1–16

Ritchie DG, Garcia JP, Amaya F, Jefferies MG (2003) Curtain grouting for the Antamina Dam, Peru: part 2—implementation and field modifications. In: Grouting and ground treatment. ASCE, pp 929–940

Shen SL, Wang ZF, Horpibulsuk S, Kim YH (2013a) Jet-grouting with a newly developed technology: the twin-jet method. Eng Geol 152(1):87–95

Shen SL, Wang ZF, Yang J, Ho EC (2013b) Generalized approach for prediction of jet grout column diameter. J Geotech Geoenviron 139(12):2060–2069

Shen SL, Wu HN, Cui YJ, Yin ZY (2014) Long-term settlement behavior of metro tunnels in the soft deposits of Shanghai. Tunn Undergr Sp Technol 40(12):309–323

Shen SL, Cui QL, Ho EC, Xu YS (2016) Ground response to multiple parallel microtunneling operations in cemented silty clay and sand. J Geotech Geoenviron 142(5):04016001

Shirlaw JN (2016) Pressurised TBM tunnelling in mixed face conditions resulting from tropical weathering of igneous rock. Tunn Undergr Sp Technol 57:225–240

Shirlaw JN, Hencher SR, Zhao J (2000) Design and construction issues for excavation and tunnelling in some tropically weathered rocks and soils. In: ISRM international symposium. International Society for Rock Mechanics

Stavropoulou M, Papanastasiou P, Vardoulakis I (1998) Coupled wellbore erosion and stability analysis. Int J Numer Anal Met 22:749–769

Stille B, Stille H, Gustafson G, Kobayashi S (2009) Experience with the real time grouting control method. Geomech Tunn 2(5):447–459

Stille H, Gustafson G, Hassler L (2012) Application of new theories and technology for grouting of dams and foundations on rock. Geotech Geol Eng 30(3):603–624

US army corps of engineers (2004) Grouting methods and equipment. UFC 3-220-06, Washington

Valko P, Economides M (1994) Propagation of hydraulically induced fractures—a continuum damage mechanics approach. Int J Rock Mech Min 31:221–229

Vardoulakis I, Stavropoulou M, Papanastasiou P (1996) Hydro-mechanical aspects of the sand production problem. Transport Porous Med 22:225–244

Wang JA, Park HD (2003) Coal mining above a confined aquifer. Int J Rock Mech Min 40:537–551

Wang Q, Qu LQ, Guo HY, Wang QS (2011) Grouting reinforcement technique of Qingdao Jiaozhou Bay subsea tunnel. Chin J Rock Mech Eng 30:790–802 **(in Chinese)**

Wu HN, Shen SL, Liao SM, Yin ZY (2015a) Longitudinal structural modelling of shield tunnels considering shearing dislocation between segmental rings. Tunn Undergr Sp Tech 50:317–323

Wu YX, Shen SL, Yin ZY, Xu YS (2015b) Characteristics of groundwater seepage with cut-off wall in gravel aquifer. II: numerical analysis 1. Can Geotech J 52(10):1539–1549

Xu YS, Shen SL, Ren DJ, Wu HN (2016) Factor analysis of land subsidence in Shanghai: a view based on strategic environmental assessment. Sustainability 8(6):573. doi:10.3390/su8060573

Yang TH, Liu J, Zhu WC, Elsworth D, Tham LG, Tang CA (2007) A coupled flow–stress–damage model for groundwater outbursts from an underlying aquifer into mining excavations. Int J Rock Mech Min 44:87–97

Yang GC, Wang XH, Wang XG, Cao YG (2016) Analyses of seepage problems in a subsea tunnel considering effects of grouting and lining structure. Mar Georesour Geotechnol 34(1):65–70

Zhang DL, Fang Q, Lou HC (2014a) Grouting techniques for the unfavorable geological conditions of Xiang'an subsea tunnel in China. J Rock Mech Geotech Eng 6(5):438–446

Zhang R, Jiang ZQ, Zhou HY, Yang CW, Xiao SJ (2014b) Groundwater outbursts from faults above a confined aquifer in the coal mining. Nat Hazards 71:1861–1872

Zhang QS, Li P, Wang G, Li SC, Zhang X, Zhang QQ, Wang Q, Liu JG (2015) Parameters optimization of curtain grouting reinforcement cycle in Yonglian tunnel and its application. Math Probl Eng 2015:15. doi:10.1155/2015/615736

Zhao J, Gong QM, Eisensten Z (2007) Tunnelling through a frequently changing and mixed ground: a case history in Singapore. Tunn Undergr Sp Technol 22(4):388–400

Zhao Y, Li P, Tian S (2013) Prevention and treatment technologies of railway tunnel water inrush and mud gushing in China. J Rock Mech Geotech Eng 5(6):468–477

Zhu WC, Wei CH (2011) Numerical simulation on mining-induced water inrushes related to geologic structures using a damage-based hydromechanical model. Environ Earth Sci 62(1):43–54